Solar Phys (2014) 289:2269–2281
DOI 10.1007/s11207-013-0447-9

The Ten-Rotation Quasi-periodicity in Sunspot Areas

R. Getko

Received: 25 September 2009 / Accepted: 31 October 2013 / Published online: 22 November 2013

Abstract Sunspot-area fluctuations over an epoch of 12 solar cycles (12 – 23) are investigated in detail using wavelets. Getko (*Universal Heliophysical Processes, IAU Symp.* **257**, 169, 2009) found three significant quasi-periodicities at 10, 17, and 23 solar rotations, but two longer periods could be treated as subharmonics of the ten-rotation quasi-periodicity. Therefore we focused the analysis on the occurrence of this quasi-periodicity during the low- and high-activity periods of each solar cycle. Because of the N – S asymmetry, each solar hemisphere was considered separately. The skewness of each fluctuation-probability distribution suggests that the positive and negative fluctuations could be examined separately. To avoid the problem that occurs when a few strong fluctuations create a wavelet peak, we applied fluctuation transformations for which the amplitudes at the high- and the low-activity periods are almost the same. The wavelet analyses show that the ten-rotation quasi-periodicity is mainly detected during the high-activity periods, but it also exists during a few low-activity periods. The division of each solar hemisphere into 30°-wide longitude bins and the wavelet calculations for the areas of sunspot clusters belonging to these 30° bins enable one to detect longitude zones in which the ten-rotation quasi-periodicity exists. These zones are present during the whole high-activity periods and dominate the integrated spectra.

Keywords Sunspot activity fluctuations · Wavelet transform

1. Introduction

In the past few decades, mid-term quasi-periodicities of many solar-activity tracers have been discussed. Wolff (1983) reported the periodicity of about 12 rotations in the monthly Wolf-number variations from 1749 to 1979. This periodicity was also found in many solar-activity indicators. Delache, Laclare, and Sadsoud (1985) detected it in the solar-diameter

R. Getko (✉)
Astronomical Institute, University of Wrocław, Kopernika 11, 51-622 Wrocław, Poland
e-mail: getko@astro.uni.wroc.pl

measurements during Cycle 21. Lean and Brueckner (1989) found it in the power spectrum of the sunspot-blocking function, in the 10.7-cm radio flux, the sunspot number, and in the plage-index daily data during three solar cycles (19 – 21). Pap, Tobiska, and Bouwer (1990) showed that an 8 – 11 month period existed in the total and UV irradiances (1980 and 1982 – 1988, respectively), in the 10.7-cm radio flux (1947 – 1989), the Ca K plage index (1970 – 1987), the sunspot blocking function (1874 – 1982), and the Mg II core–wing ratio (1978 – 1986). Akioka *et al.* (1987) detected it in areas and numbers of sunspot groups from 1969 to 1986. Oliver, Carbonell, and Ballester (1992) studied daily sunspot numbers from Solar Cycles 6 – 21. They adopted two different power-spectral methods and found a periodicity of about 323 days in three solar cycles alone. They also found a significant periodicity at 350 days (13 rotations) during Cycles 12 – 21 together and in some individual cycles. Getko (2006) found a statistically significant quasi-periodicity of about nine months (ten rotations) in both high- and low-activity periods for the monthly Wolf-number fluctuations from Solar Cycles 1 – 22 and for the group-sunspot number fluctuations from Solar Cycles 5 – 22.

Two longer periods at 17 and 23 rotations were found in many solar-activity parameters. A more up-to-date review is given by Obridko and Shelting (2007). Recently, Getko (2009) showed that these periods could be treated as subharmonics of the ten-rotation period. This was able to explain a wide range of periodicities in various solar indices at all levels from the tachocline to Earth.

In this article, the occurrence of the ten-rotation quasi-periodicity in the sunspot areas during the low- and high-activity periods for Cycles 12 – 23 is studied. The N – S asymmetry of solar activity (Vizoso and Ballester, 1990) suggests that the two hemispheres should be considered separately. It is known that for a time series that contains Gaussian white noise and a sinusoidal component, the probability distribution is symmetric and the autocorrelation functions $[c_\tau]$ of that time series, of its positive fluctuations, and of its negative fluctuations should be the same. Getko (2009) showed that these c_τ-functions for one solar cycle are different. Therefore the positive and the negative fluctuations are considered separately. To avoid the problem that occurs when a few strong fluctuations create a wavelet peak, we applied a transformation of each fluctuation time series into a new time series that has a constant variance (Getko, 2006). The amplitudes of these new time series at the high- and the low-activity periods are almost the same. The wavelet analyses of the original fluctuations and their transformations were used to find the mid-term periodicities from high- and low-activity periods in each solar cycle. To associate these results with the observed features on the solar surface, we evaluated the longitude distributions of sunspot-group clusters that are close to one another and that create the strong sunspot-area fluctuations that existed during each solar cycle in each solar hemisphere. Because these clusters have a longitudinal extent of up to 30°, the solar disk was divided into 30°-wide longitude bins. For each longitude bin the new sunspot-area time series was considered. It contains all sunspot groups or sunspot-group clusters that existed during each solar cycle. Its wavelet analysis determines the time intervals where the mid-term periodicities exist.

2. The Stationary Version of Sunspot Area Fluctuations

The daily sunspot areas for the northern hemisphere $[D_i^n]$ and the southern hemisphere $[D_i^s]$ for Solar Cycles 12 – 23 are available from the National Data Geophysical Center (NGDC) [http://solarscience.msfc.nasa.gov/greenwch/]. For the ith Carrington rotation the mean area

for the northern hemisphere $[S_i^n]$ is given by the expression

$$S_i^n = \frac{1}{K}\sum_{l=1}^{K} D_l^n,$$

where K is the number of days for the ith rotation. The fluctuation $[F_i^n]$ of the mean area $[S_i^n]$ from the smoothed mean area is defined as

$$F_i^n = S_i^n - \overline{S_i^n} \quad \text{for } i = 1, \ldots, N,$$

where $\overline{S_i^n} = \frac{1}{13}\sum_{j=i-6}^{i+6} S_i^n$. Each of $\{F_i^n\}$ and $\{F_i^s\}$ contains $N = 1706$ elements. The beginning and the end of each cycles is defined by the minima of the smoothed monthly Wolf numbers. Each time series has zero mean value and time-dependent variance. To stabilize the variance, the procedure shown by Getko (2006) in the appendix was applied. For the ith rotation the value $[X_i^n]$ of the new time series $\{X_i^n\}_{i=1}^N$ is a function of two parameters k and u (see Equation (A.2) in the appendix of Getko, 2006). The values k and $\log A$ are estimated from Equation (A.10) of Getko (2006). The best solution is found for $u = 13$ (rotations) and $k = 0.68 \pm 0.02$. For $\{F_i^s\}$ it is found for $u = 13$ (rotations) and $k = 0.83 \pm 0.02$. The two coefficients k are statistically significant at the 95 % confidence level (the F-statistic was used).

To verify the stationarity conditions of $\{X_i^n\}$ and $\{X_i^s\}$, their means $[\overline{\mathcal{X}} = \frac{1}{u}\sum_{j=i_1-[\frac{u}{2}]}^{i_1+[\frac{u}{2}]} X_j]$, standard deviations $[\overline{\boldsymbol{\sigma}} = \sqrt{\frac{1}{u}\sum_{j=i_1-[\frac{u}{2}]}^{i_1+[\frac{u}{2}]} (X_j - \overline{\mathcal{X}})^2}]$, and auto-correlation functions $[c_\tau]$ were computed. For each time series about 70 % of the values of $\overline{\mathcal{X}}$ for $u = 13$ and $i_1 = 7, 20, \ldots, 1698$ belong to the interval $(\overline{\mathcal{X}} - \widehat{\sigma}, \overline{\mathcal{X}} + \widehat{\sigma})$, where $\overline{\mathcal{X}^n} \approx -0.15$, $\widehat{\sigma^n} \approx 0.7$, $\overline{\mathcal{X}^s} \approx -0.08$, and $\widehat{\sigma^s} \approx 0.3$. All sample standard deviations for each time series belong to the interval $(\overline{\boldsymbol{\sigma}} - 2\widehat{\sigma}, \overline{\boldsymbol{\sigma}} + 2\widehat{\sigma})$, where $\overline{\boldsymbol{\sigma}^n} \approx 4.4$, $\widehat{\sigma^n} \approx 0.4$, $\overline{\boldsymbol{\sigma}^s} \approx 1.8$, and $\widehat{\sigma^s} \approx 0.2$. The c_τ-functions of $\{X_i\}$, $\{X_i^o\}$, and $\{X_i^*\}$ for all 12 cycles for the northern and the southern hemispheres were also considered. Here $\{X_i^o\}$ and $\{X_i^*\}$ were computed after dividing $\{X_i\}_{i=1}^N$ into two parts: those from the periods of high- and low-sunspot activities, respectively. To evaluate these periods, the smoothed monthly Wolf numbers $[\{\overline{R_m}\}_{m=1}^{N_1}]$ were used. All m for which the values $\overline{R_m}$ are lower (higher) than the mean value of $\{\overline{R_m}\}$ define low- (high-)activity periods. For each c_τ two standard errors were calculated. Because each of the three time series has a different length $[M]$, the bounds for the shortest time series were used (± 0.068). The differences between the c_τ-functions of $\{X_i^{no}\}$ and $\{X_i^{n*}\}$ are larger than 2σ for $\tau = 11, 13, 16, 17, 20, 25, 33,$ and 34 rotations. For the southern hemisphere the two c_τ-functions differ significantly at $\tau = 7, 10, 12, 15, 19, 23, 30,$ and 34 rotations. Although the means and the standard deviations of $\{X_i\}$, $\{X_i^o\}$, and $\{X_i^*\}$ are approximately constant, the c_τ-functions are different. Thus, $\{X_i^n\}$ and $\{X_i^s\}$ are not stationary.

Because each fluctuation-probability distribution has positive skew (Getko, 2009), the positive and negative fluctuations were considered separately. For $\{F_i^n\}$ they can be defined as follows:

$$F_i^{n+} = \begin{cases} 0 & \text{where } F_i^n \le 0 \\ F_i^n & \text{where } F_i^n > 0 \end{cases} \quad \text{for } i = 1, \ldots, N,$$

$$F_i^{n-} = \begin{cases} 0 & \text{where } F_i^n > 0 \\ F_i^n & \text{where } F_i^n \le 0 \end{cases} \quad \text{for } i = 1, \ldots, N.$$

The same definitions were applied to X_i^{n+} and X_i^{n-}, and to all these time series for the southern hemisphere.

3. The Periodicities During High- and Low-Activity Periods

To find the periodicities during high-activity periods, the original, the positive, and the negative fluctuations were considered separately. The same procedure was applied for transformations. For example, for the northern hemisphere the following time series were considered: $\{F_i^n\}_{i=1}^N$, $\{X_i^n\}_{i=1}^N$, $\{F_i^{n+}\}_{i=1}^N$, $\{X_i^{n+}\}_{i=1}^N$, $\{F_i^{n-}\}_{i=1}^N$, and $\{X_i^{n-}\}_{i=1}^N$. The Morlet wavelet (Torrence and Compo, 1998) was applied to these time series for each of the solar hemispheres. The wavelet maps for fluctuations and their transformations are presented in Figures 1 – 6. For fluctuations $\{F_i^n\}$ and $\{F_i^s\}$ the wavelet maps show statistically significant peaks at $\tau \in [7, 13]$ rotations. No single periodicity from this time interval seems to be favored. The peaks are always present during the high-activity periods. They extend in time up to 25 solar rotations and dominate the integrated spectra. Their global maxima are at $\tau =$ ten and nine rotations for $\{F_i^n\}$ and $\{F_i^s\}$, respectively. For the positive fluctuations, the significant local maxima of wavelets for $\tau \in [7, 13]$ rotations are almost the same as for the fluctuations. For negative fluctuations there are more such maxima. They also exist during a few low-activity periods. For positive fluctuations the global maxima of integrated spectra are wider and lower than for fluctuations. For negative fluctuations each integrated spectrum has one strong and narrow peak. An analysis of integrated spectra calculated for each solar hemisphere and for each solar cycle separately indicates that this effect exists for about 70 % of the cases. Thus, the time distances between fluctuation minima are more concentrated around the mean value than for fluctuation maxima.

To find the periodicities during the low-activity periods, the wavelets of $\{X_i^n\}$ and $\{X_i^s\}$ for 12 cycles together are examined. After these transformations, the weak and strong fluctuations have the same amplitude. This makes it possible to find the periodicity that occurs during the low-activity periods. The map of $\{X_i^{n+}\}$ shows significant peaks at about ten rotations from these periods (Cycles 13 – 14, 15 – 16, 17 – 18, and 20 – 21). For $\{X_i^{n-}\}$ there are also several significant peaks (Cycles 13 – 14, 16 – 17, 17 – 18, 18 – 19, and 20 – 21). Both maps of $\{X_i^{s+}\}$ and $\{X_i^{s-}\}$ also show significant peaks during these periods (Cycles 12 – 13, 13 – 14, 15 – 16, 16 – 17, 18 – 19 and Cycles 12 – 13, 15 – 16, 16 – 17 respectively).

Shorter periodicities (for $\tau <$ seven rotations) were also studied. They are only occasionally present in all wavelet maps. Their duration is shorter than that of the ten-rotation quasi-periodicity.

To combine the wavelet results with the observed features on the solar surface, we evaluated the longitude distribution of sunspot-group clusters that create the strong sunspot-area fluctuations that existed during each of the 12 solar cycles in each solar hemisphere (24 cases). A similar method was introduced by Getko (2004). Firstly, for each case a set of strong positive fluctuations is defined. Because the empirical distributions of each fluctuation time series is not normal, the three-σ rule should not be used. Therefore we applied a method that supplies the best value of the parameter p such that the fluctuation (for example, for the northern hemisphere) $F_i^n > p$ could be treated as a strong fluctuation (Getko, 2004). After a detailed analysis of 24 cases, the parameter p for each case was determined. It is one σ, where σ is the empirical standard deviation of each fluctuation time series. Next, for each ith rotation (such that $F_i^n > p$) the mean positions and the rotational sum of each sunspot group areas were calculated. We found all clusters created by large groups and all smaller groups that are close to one another (Getko, 2013). For these clusters, the weighted positions of the area and total areas were evaluated. Almost all clusters have a longitudinal extent of up to 30° (Getko, 2007). To obtain their longitude distribution, the solar disk was divided into 30°-wide longitude bins. For each bin we determined the number of clusters. To avoid a phase-shift problem, we considered thirty histograms made such that their first

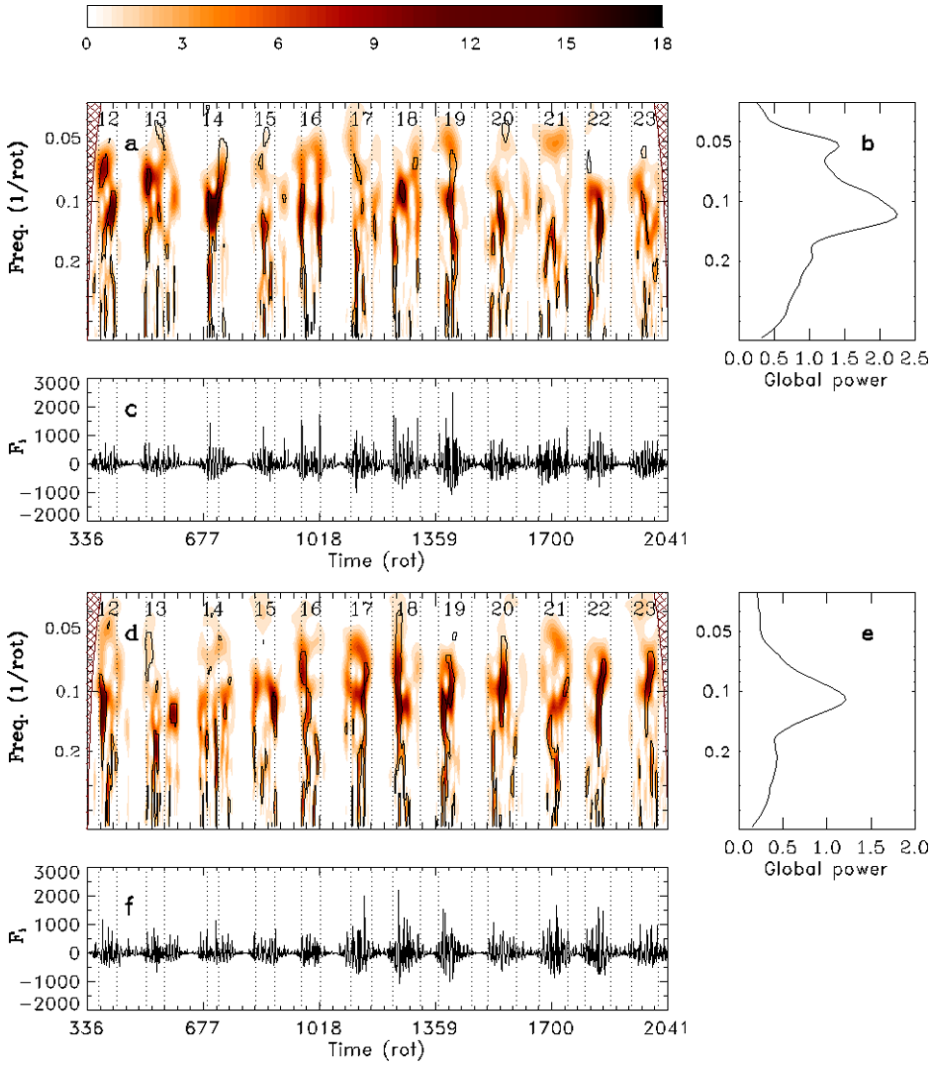

Figure 1 (a) Wavelet power spectrum of $\{F_i^n\}$ for Cycles 12 – 23 mapping a time–frequency evolution of about ten-rotation periodicity. Top values of wavelet power are denoted by gradual darkening. Black contours denote significance levels of 95 % for detected peaks. A cone of influence is marked as a dashed region. (b) Corresponding global wavelet power spectrum. (c) Time series $\{F_i^n\}$ for Cycles 12 – 23. (d) – (f) same as (a) – (c), but for $\{F_i^s\}$.

bin started from 0° to 29° every 1°. For each of them we calculated the sum of the squares of the deviations of the empirical frequencies from the uniform-distribution values. For the best histogram this sum is to be larger than from any other histogram. This longitude separation provided 12 time series, each of which contains the total areas of all the clusters and all other sunspot groups (which do not create clusters) occurring in the 30-degree bin. To find the mid-term periodicities for each longitude bin, we applied the wavelet analysis.

Figures 7a and 7b show the behavior of the ten-rotation quasi-periodicity during Cycles 12 – 23 for 30°-wide longitude bins of the northern and the southern hemisphere, re-

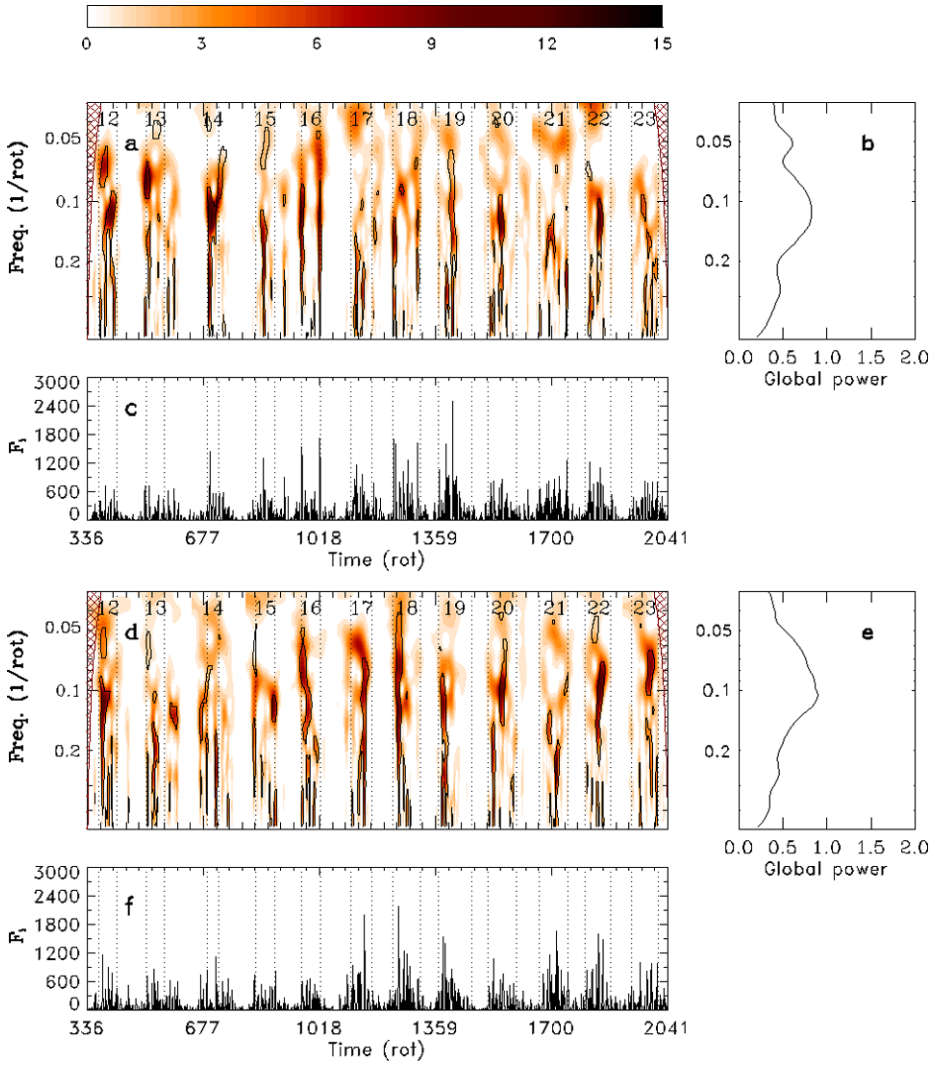

Figure 2 (a) Wavelet power spectrum of $\{F_i^{n+}\}$ for Cycles 12 – 23 mapping a time–frequency evolution of about ten-rotation periodicity. Top values of wavelet power are denoted by gradual darkening. Black contours denote significance levels of 95 % for detected peaks. A cone of influence is marked as a dashed region. (b) Corresponding global wavelet power spectrum. (c) Time series $\{F_i^{n+}\}$ for Cycles 12 – 23. (d) – (f) same as (a) – (c), but for $\{F_i^{s+}\}$.

spectively. For these bins the statistically significant peaks of wavelet maps indicate this quasi-periodicity and the time intervals $[t_1, t_2]$ where they exist. Each horizontal segment connecting two points represents the time intervals where the periodicities of $\tau \in [7, 13]$ rotations are found. Note that for all 24 cases the ten-rotation quasi-periodicity exists during each high-activity period. Moreover, the time intervals are much longer than the intervals that are found for the whole solar hemispheres (see Figures 1a and 1d). Moreover, this periodicity can be found in the low-activity periods (Cycles 11 – 12, 12 – 13, 13 – 14, 14 – 15, 15 – 16, 16 – 17, 17 – 18, 19 – 20, 20 – 21, 22 – 23, and 23 – 24 in the northern hemisphere

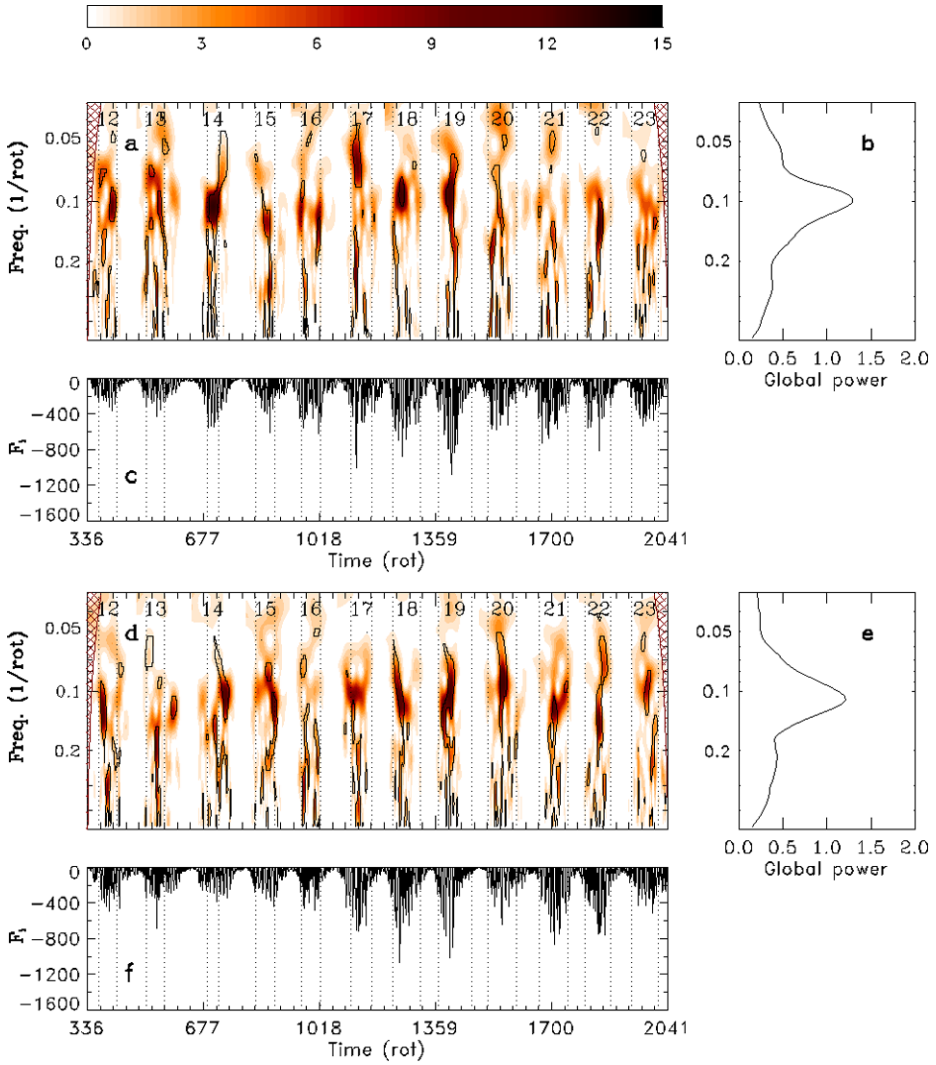

Figure 3 (a) Wavelet power spectrum of $\{F_i^{n-}\}$ for Cycles 12 – 23 mapping a time–frequency evolution of about ten-rotation periodicity. Top values of wavelet power are denoted by gradual darkening. Black contours denote significance levels of 95 % for detected peaks. A cone of influence is marked as a dashed region. (b) Corresponding global wavelet power spectrum. (c) Time series $\{F_i^{n-}\}$ for Cycles 12 – 23. (d) – (f) same as (a) – (c), but for $\{F_i^{s-}\}$.

and Cycles 11 – 12, 12 – 13, 13 – 14, 14 – 15, 15 – 16, 16 – 17, 20 – 21, 22 – 23, and 23 – 24 in the southern hemisphere). It is very likely that this periodicity also occurs in other low-activity periods, because the wavelet maps show statistically insignificant strips of increased values at this quasi-periodicity.

Figures 8a and 8b present the longitude distributions of this quasi-periodicity (from Figures 7a and 7b) in time for the northern and the southern hemisphere, respectively. In all 24 cases one can find very wide longitude zones from 60° to 330° (during Cycle 18 in the northern hemisphere almost all 30°-wide longitude bins show the ten-rotation quasi-

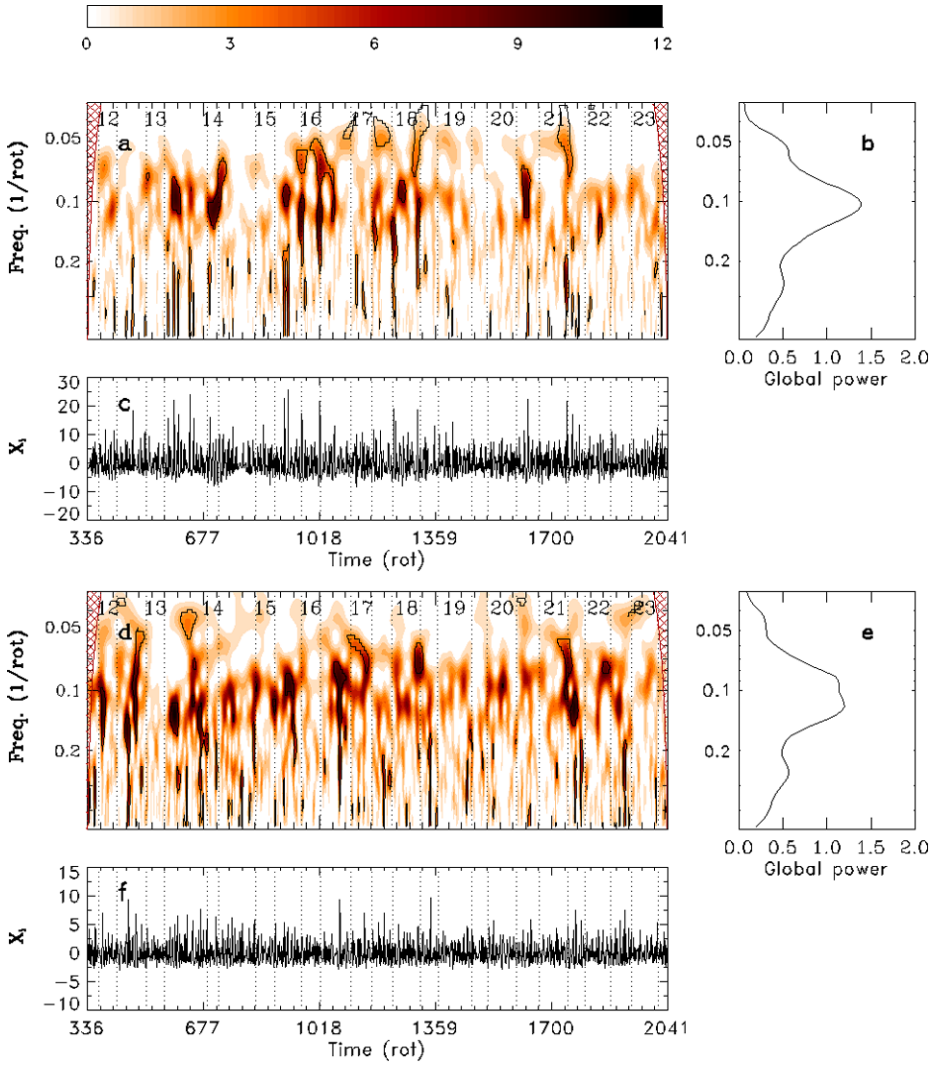

Figure 4 (a) Wavelet power spectrum of $\{X_i^n\}$ for Cycles 12 – 23 mapping a time–frequency evolution of about ten-rotation periodicity. Top values of wavelet power are denoted by gradual darkening. Black contours denote significance levels of 95 % for detected peaks. A cone of influence is marked as a dashed region. (b) Corresponding global wavelet power spectrum. (c) Time series $\{X_i^n\}$ for Cycles 12 – 23. (d) – (f) same as (a) – (c), but for $\{X_i^s\}$.

periodicity). In these zones the ten-rotation quasi-periodicity lasts from 53 rotations (Cycle 17 in the northern hemisphere) to 97 rotations (Cycle 23 in the southern hemisphere). In these situations it exists in one 30° bin during a few or several rotations and then appears in neighboring bins. At the same time, there may exist from one to four quasi-periodical longitude zones. Note that these periodicities and time intervals $[t_1, t_2]$ were obtained for the whole hemisphere data (see Figures 1a and 1d), for which any longitude bins and any periodicities that existed during these time intervals cannot be found. These cases could be a spurious effect.

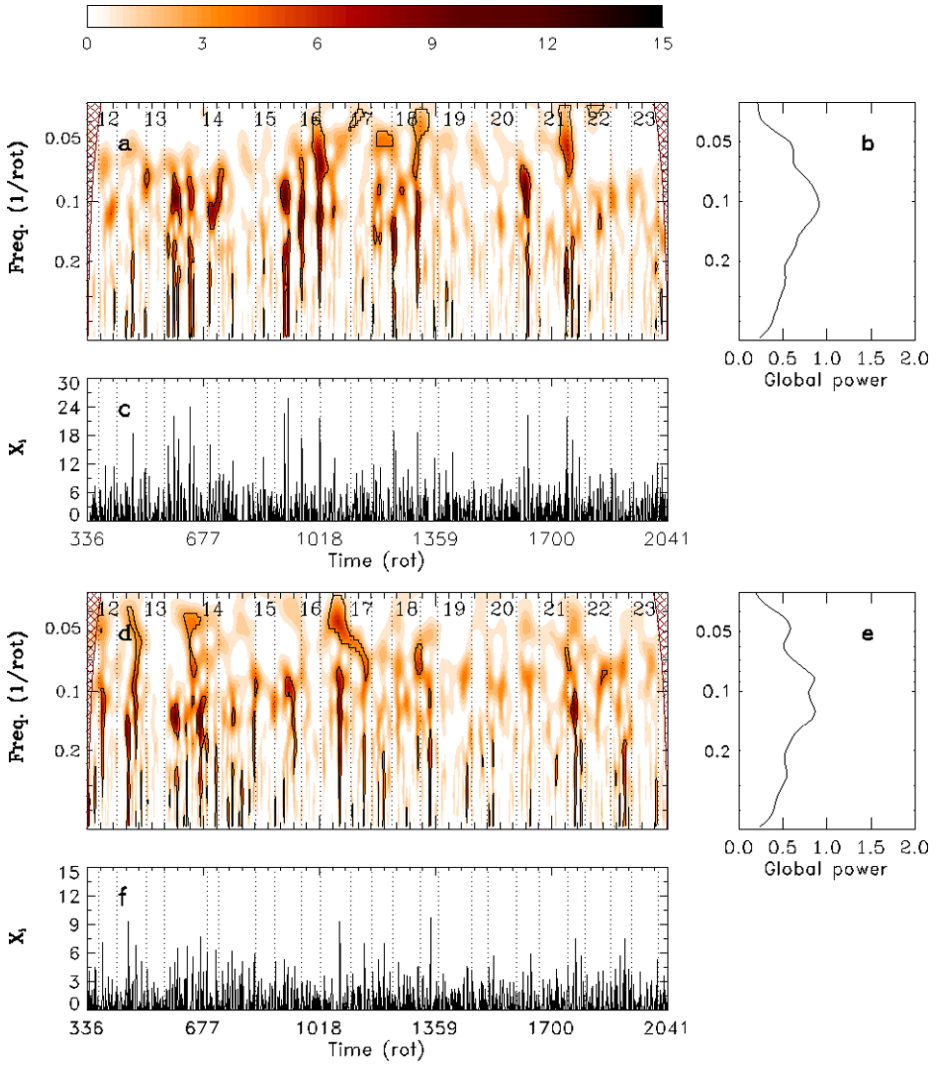

Figure 5 (a) Wavelet power spectrum of $\{X_i^{n+}\}$ for Cycles 12 – 23 mapping a time–frequency evolution of about ten-rotation periodicity. Top values of wavelet power are denoted by gradual darkening. Black contours denote significance levels of 95 % for detected peaks. A cone of influence is marked as a dashed region. (b) Corresponding global wavelet power spectrum. (c) Time series $\{X_i^{n+}\}$ for Cycles 12 – 23. (d) – (f) same as (a) – (c), but for $\{X_i^{s+}\}$.

4. Discussion

The ten-rotation quasi-periodicity was previously detected for the whole-solar-disk data. Getko (2006) obtained it for the monthly Wolf numbers and for the sunspot-group numbers during high-activity periods. Prabhakaran Nayar *et al.* (2002) showed a significant wavelet power of the daily Wolf numbers at periods around 11 – 12 rotations for short time-intervals during several solar maxima. The auto-correlation and the wavelet analyses of rotational data for each solar hemisphere confirmed the dominance of this periodicity (Getko, 2009).

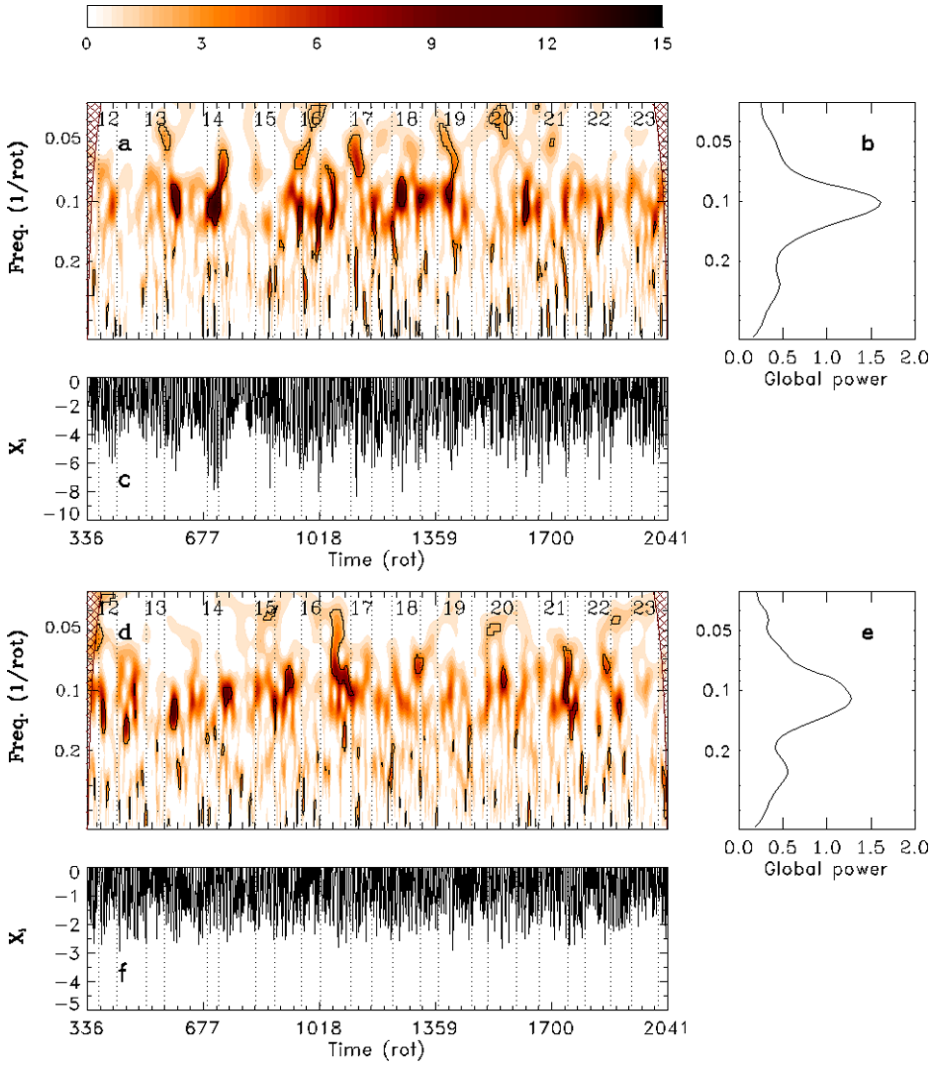

Figure 6 (a) Wavelet power spectrum of $\{X_i^{n-}\}$ for Cycles 12 – 23 mapping a time–frequency evolution of about ten-rotation periodicity. Top values of wavelet power are denoted by gradual darkening. Black contours denote significance levels of 95 % for detected peaks. A cone of influence is marked as a dashed region. (b) Corresponding global wavelet power spectrum. (c) Time series $\{X_i^{n-}\}$ for Cycles 12 – 23. (d) – (f) same as (a) – (c), but for $\{X_i^{s-}\}$.

Taking into consideration that the solar-activity fluctuations are quasi-periodical, the results obtained for daily, monthly, and rotational data are similar. In this article each solar hemisphere was considered separately and an attempt was undertaken to find the time intervals and the longitude zones in which this quasi-periodicity exists.

Firstly, the transformation of both fluctuation time series into the new time series with a constant variance enables one to evaluate the time intervals where the mid-term periods are dominant. Such analyses for each solar hemisphere indicate that the mean time interval

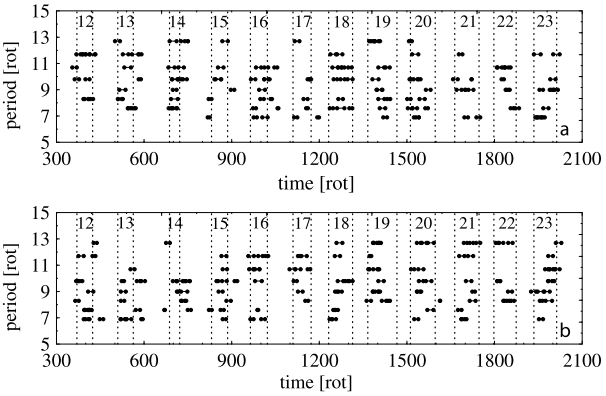

Figure 7 (a) Behavior of the northern hemispheric ten-rotation quasi-periodicity for Cycles 12 – 23. Vertical dotted lines show the high- and the low-activity periods. The cycle numbers are given for all high-activity periods. (b) Same as for (a), but for the southern hemisphere.

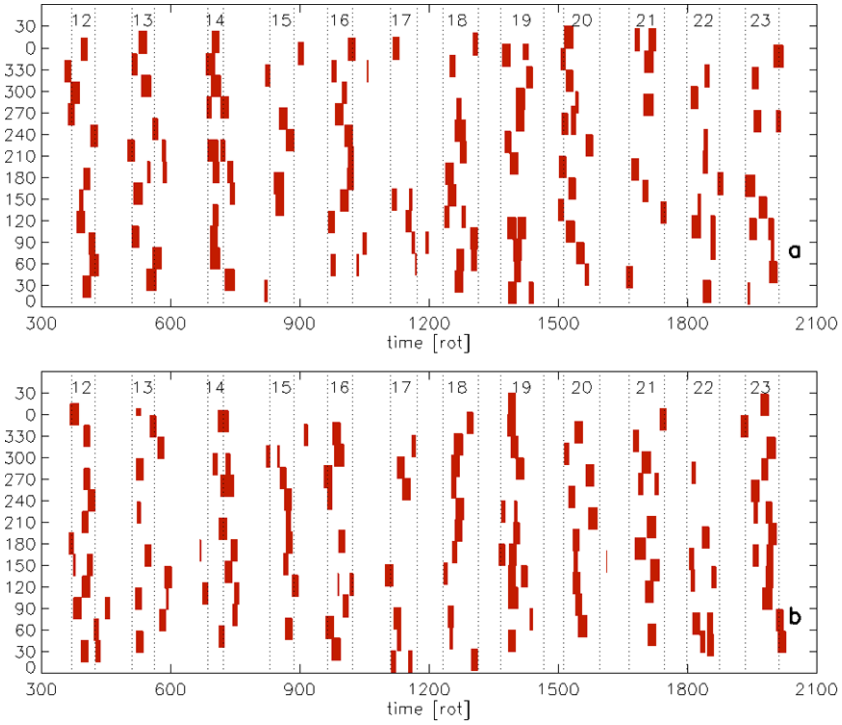

Figure 8 (a) Filled areas demonstrate the presence of the northern hemispheric ten-rotation quasi-periodicity in 30°-wide longitude bins during Cycles 12 – 23. Vertical dotted lines show the high- and the low-activity periods. The cycle numbers are given for all high-activity periods. (b) Same as for (a), but for the southern hemisphere.

between strong fluctuations from solar maxima is about ten rotations. Moreover, the division of $\{X_i\}$ for each hemisphere into two shorter parts, containing data from low-activity periods $[\{X_i^*\}]$ and from high-activity periods $[\{X_i^o\}]$, enables one to verify possible differences between periodicities existing during these periods in 12 solar cycles. For each hemisphere the functions c_τ of all three of these time series have wide global maxima at $\tau \in [7, 13]$

rotations. The functions c_τ of $\{X_i^n\}$ and $\{X_i^{n*}\}$ have a significant global maxima at $\tau =$ eleven rotations, but for $\{X_i^{no}\}$ two local maxima at eight and ten rotations are between 1σ and 2σ. For the southern hemisphere all three global maxima are greater than 2σ. For $\{X_i^{so}\}$ this maximum contains two peaks that are almost the same at $\tau =$ eight and ten rotations.

Then, to confirm these results, the wavelet analysis was applied to all time series. All global spectra have the dominant peaks at $\tau =$ ten rotations. For $\{X_i^{n+}\}$ and $\{X_i^{s+}\}$ these peaks are much wider and lower than for $\{X_i^{n-}\}$ and $\{X_i^{s-}\}$. These wide maxima indicate that the time separations between fluctuation maxima oscillate around an average length τ. This fact could be caused by the differential rotation and the different rotation rate of activity complexes during their life time (Gaizauskas *et al.*, 1983). In addition, Getko (2004) showed that strong positive fluctuations are always created by two to four activity complexes that do not have their largest size at the same time (the maxima of their contribution to the monthly Wolf number are shifted from one to three months). Namely, the fluctuations are not strictly periodic, but quasi-periodic. Moreover, because the wavelets of positive and negative fluctuations are different, the positive fluctuations, which describe strong magnetic-flux emergence, are more a sequence of pulses following at fixed time intervals than harmonic oscillations (Obridko and Shelting, 2007). In addition, for $\{F_i^{n+}\}$ and $\{F_i^{s+}\}$ the significant wavelet peaks at ten rotations typically exist during short time-intervals of high-activity periods and also exist in the maps of $\{X_i^{n+}\}$ and $\{X_i^{s+}\}$ during several low-activity periods.

Finally, all of the above results were confirmed by the wavelet analysis of sunspot-cluster areas calculated for the 30°-wide longitude bins. During almost every rotation of all high-activity periods, there are up to four longitude zones that show the ten-rotation quasi-periodicity. Moreover, this periodicity was also detected during a few low-activity periods. The quasi-periodic longitude zones were extended from 30° to 330°. For these larger longitude zones the ten-rotation quasi-periodicity was always detected in one 30° bin during up to 32 rotations (Cycle 14 in the northern hemisphere) and then appeared in the neighboring bins. The total lifetime of these larger longitude zones during the whole solar cycle is up to 97 rotations (Cycle 23 in the southern hemisphere). Gaizauskas *et al.* (1983) also concluded that some complexes form diverging branches with their own rotation rates. We also pointed out that the mean rotational longitude is very stable during its lifetime for each cluster that creates an active longitude. This means that their positions do not significantly change and the rotation rate of these structure does not influence the results obtained.

5. Conclusions

The following results have been obtained:

i) The wavelet analyses of the original, the positive, and the negative fluctuations and their transformations support the ten-rotation quasi-periodicity during all solar cycles in each solar hemisphere.
ii) In the wavelet maps of fluctuations, the statistically significant power values at $\tau \in [7, 13]$ rotations exist from a few to 25 rotations during each high-activity period in each solar hemisphere and dominate the integrated spectra.
iii) The separation of each solar hemisphere into 30°-wide longitude bins and the wavelet calculations for the areas of sunspot clusters belonging to these 30° bins enabled us to detect from one to four quasi-periodic longitude zones at the same time. They are present during the high-activity periods (from 53 rotations for Cycle 17 in the northern hemisphere to 97 rotations for Cycle 23 in the southern hemisphere).

iv) It is difficult to find one or more quasi-periodic longitude zones that exist during the whole high-activity period.
v) The wavelet maps of $\{X_i^{n+}\}$, $\{X_i^{n-}\}$, $\{X_i^{s+}\}$, and $\{X_i^{s-}\}$ for all 12 solar cycles together show several statistically significant peaks at about ten rotations for low-activity periods. Moreover, the wavelets of the sunspot cluster areas from the 30°-longitude bins confirm these results. This means that during these periods small quasi-periodic fluctuations exist.

References

Akioka, M., Kubota, J., Suzuki, M., Ichimoto, K., Tohmura, I.: 1987, *Solar Phys.* **112**, 313. doi:10.1007/BF00148785.
Delache, P., Laclare, F., Sadsoud, H.: 1985, *Nature* **317**, 416. doi:10.1038/317416a0.
Gaizauskas, V., Harvey, K.L., Harvey, J.W., Zwaan, C.: 1983, *Astrophys. J.* **265**, 1056. doi:10.1086/160747.
Getko, R.: 2004, *Solar Phys.* **224**, 291. doi:10.1007/s11207-005-5718-7.
Getko, R.: 2006, *Solar Phys.* **238**, 187. doi:10.1007/s11207-006-0112-7.
Getko, R.: 2007, *Adv. Space Res.* **40**, 981. doi:10.1016/j.asr.2007.02.094.
Getko, R.: 2009, In: Gopalswamy, N., Webb, D. (eds.) *Universal Heliophysical Processes, IAU Symp.* **257**, Cambridge University Press, Cambridge, 169. doi:10.1017/S174392130902924X.
Getko, R.: 2013, *J. Space Weather Space Clim.* **3**, A09. doi:10.1051/swsc/2013032.
Lean, J.L., Brueckner, G.E.: 1989, *Astrophys. J.* **337**, 568. doi:10.1086/167124.
Obridko, V.N., Shelting, B.D.: 2007, *Adv. Space Res.* **40**, 1006. doi:10.1016/j.asr.2007.04.105.
Oliver, R., Carbonell, M., Ballester, J.L.: 1992, *Solar Phys.* **137**, 141. doi:10.1007/BF00146580.
Pap, J., Tobiska, W.K., Bouwer, S.D.: 1990, *Solar Phys.* **129**, 165. doi:10.1007/BF00154372.
Prabhakaran Nayar, S.R., Radhida, V.N., Revathy, K., Ramadas, V.: 2002, *Solar Phys.* **208**, 359. doi:10.1023/A:1020565831926.
Torrence, C., Compo, G.P.: 1998, *Bull. Am. Meteorol. Soc.* **79**, 61.
Vizoso, G., Ballester, J.L.: 1990, *Astron. Astrophys.* **229**, 540.
Wolff, C.L.: 1983, *Astrophys. J.* **264**, 667. doi:10.1086/160640.